

pubs.acs.org/cm Article

Polyol Synthesis of Pd Icosahedral Nanocrystals: Insights into the Growth Mechanism and Size Control

Siyu Zhou, Chenxiao Wang, and Younan Xia*



Cite This: Chem. Mater. 2022, 34, 5065-5073



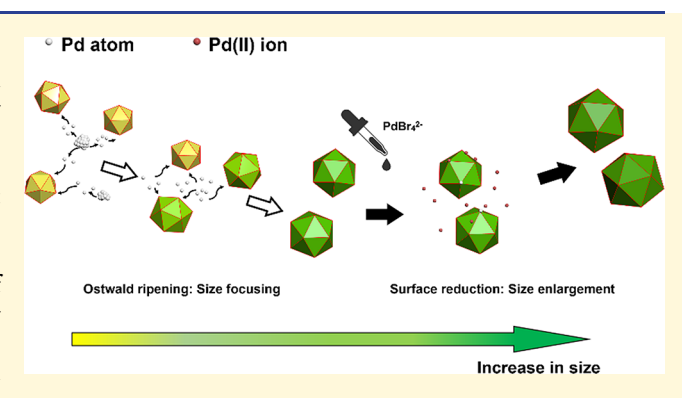
ACCESS I

Metrics & More



Supporting Information

ABSTRACT: We report a polyol method based on diethylene glycol for the synthesis of Pd icosahedral nanocrystals with uniform sizes controllable in the range of 7–20 nm. Our mechanistic study indicates that Ostwald ripening plays a vital role in the homogeneous nucleation and growth of Pd icosahedral nanocrystals with uniform sizes. As a result of the "size focusing" effect facilitated by Ostwald ripening, the broad distribution in size can be quickly narrowed to generate uniform particles with sizes up to 11 nm depending on the reduction kinetics and duration of reaction time. To obtain particles with larger sizes, one has to rely on seed-mediated growth, with the uniform icosahedral nanocrystals obtained through Ostwald ripening serving as the seeds. In such a synthesis, it is vital to suppress homogeneous nucleation while



promoting heterogeneous nucleation and layer-by-layer growth. Experimentally, this condition can be accomplished by adding a $PdBr_4^{2-}$ solution in one shot for the production of Pd icosahedral nanocrystals with uniform sizes up to 20 nm. The size can be tuned by simply controlling the growth time and/or the amount of the precursor involved in the growth step. These strategies built upon the mechanistic understanding are expected to be extendable to other noble metals, providing a robust and viable route to the synthesis of icosahedral nanocrystals with uniform sizes controllable over a broad range for fundamental studies and catalytic applications.

INTRODUCTION

Metal nanocrystals have received considerable attention for their fascinating properties as well as diverse applications related to catalysis, photonics, electronics, sensing, imaging, and medicine. Those with an icosahedral shape, in particular, have been a subject of intense research owing to their unique features, including their size-dependent strain field and the presence of a large number of twin boundaries on their surface. As demonstrated by multiple examples, these features can be leveraged to enhance their catalytic activity toward a wide variety of reactions. $^{10-13}$ To this end, it is critical to have tight control over their size as this parameter has strong correlations with a range of properties, including the distribution of strain field on the surface and the fraction of surface atoms situated on twin boundaries. 14-20 In general, it is necessary to have access to icosahedral nanocrystals featuring a broad range of uniform and controllable sizes in order to optimize their catalytic performance.

Based on thermodynamic arguments, metal clusters (i.e., the nuclei/seeds formed at the beginning of a synthesis) are found by theoretical calculations to take icosahedral, decahedral, and face-centered cubic (fcc) structures, respectively, as their size is increased.^{21–23} As such, the clusters are expected to grow and transform into seeds and then nanoparticles featuring icosahedral, decahedral, and cuboctahedral shapes, respec-

tively. In practice, however, both icosahedral and decahedral particles could still be obtained in a colloidal synthesis even when their size has been increased well into the region where the single-crystal fcc structure is supposed to be most stable. This deviation can be attributed to the fact that most of the reported syntheses are actually conducted under kinetic control rather than thermodynamic control. As such, multiply twinned nanoparticles can still be obtained as the products.

In literature, "multiple twinning" often refers to icosahedral and decahedral particles, both characterized by a pentatwinned internal structure but with different symmetry. Their synthesis typically involves a polyol that serves as a solvent and a reducing agent for the metal precursor.²⁴ In polyol synthesis, the twin defects can be protected from oxidative etching because of the low solubility of O₂ in polyol.²⁵ As demonstrated in the polyol synthesis of Pd nanocrystals, the internal structure taken by the seeds had a strong dependence

Received: February 7, 2022 Revised: May 18, 2022 Published: May 31, 2022





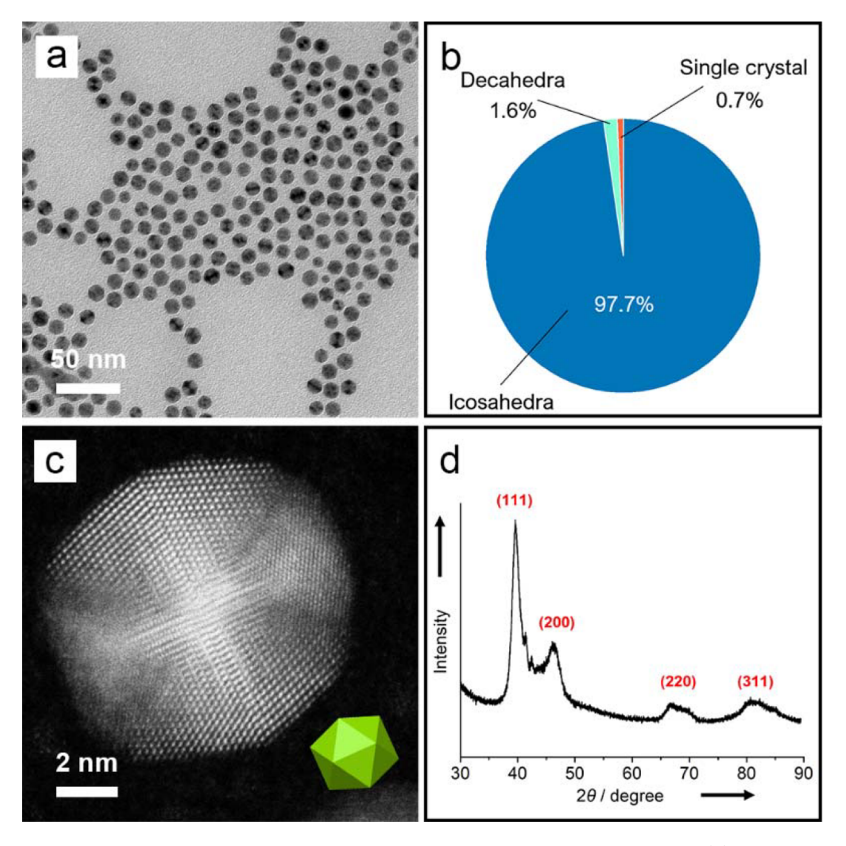


Figure 1. Characterizations of the Pd icosahedral nanocrystals prepared using the standard procedures: (a) TEM image of the as-obtained sample, (b) distribution of icosahedral, decahedral, and single-crystal particles in the sample, (c) HAADF-STEM image of an icosahedral nanocrystal oriented along the 2-fold axis, and (d) X-ray diffraction pattern. The orientation of the icosahedral nanocrystal in (c) is depicted by the model in the inset.

on the initial reduction rate of the precursor.²⁶ Specifically, as the reduction rate was slowed down, the resultant seeds would be increasingly dominated by single-crystal, singly twinned, multiply twinned (icosahedral and decahedral), and stacking fault-lined structures. By further fine-tuning the initial reduction rate, Pd icosahedral seeds can be obtained as the more favorable products over decahedral seeds. Practically, by adjusting the initial reduction rate, it is feasible to obtain nanocrystals exclusively with a multiply-twinned structure, but their sizes tend to take a broad distribution due to the involvement of multiple nucleation events. 15,27-31 According to the LaMer model, if the concentration of metal atoms cannot be quickly brought down to a level below the threshold for homogeneous nucleation, additional nucleation events can still occur in the growth step. 32 As a result, the particles in the final product would take a polydispersed distribution in terms of size, even though they might share the same internal structure.

Ostwald ripening has been recognized as an effective strategy to help improve the size uniformity of colloidal nanocrystals as a result of its "size focusing" effect. $^{33-35}$ In this thermodynamically-driven process, smaller particles are dissolved and then re-deposited onto the surface of larger ones in an effort to minimize the surface to volume ratio and thus total surface energy of the system. 36 Using Monte Carlo simulations, Talapin et al. demonstrated "size focusing" for an ensemble of growing nanocrystals via Ostwald ripening. 34 According to their modeling results, there exists a critical radius ($r_{\rm cr}$) at which the dissolution rate of a particle is equal to the growth rate. Particles with sizes smaller than $r_{\rm cr}$ automatically dissolve,

and the resultant species are then incorporated into the surface of particles larger than r_{cr} . For the particles capable of growing, the smallest one would grow at the greatest rate along the radial direction due to its smallest surface area. As a result, the size distribution will narrow over time, and eventually, all the particles are expected to reach a more or less identical size. The "size focusing" effect enabled by Ostwald ripening has also been experimentally proven in the colloidal synthesis of many types of nanoparticles, including metal oxide nanocrystals and quantum dots. 33,35,37 In a previous study, Teranishi and coworkers synthesized Pd icosahedral nanocrystals by reducing Na₂PdCl₄ with sodium chloride (NaCl) in ethylene glycol (EG), with poly(vinylpyrrolidone) (PVP) serving as a colloidal stabilizer.³⁸ In their synthesis, small particles were formed during the growth stage due to the involvement of solution reduction of PdCl₄²⁻ and, thus, homogeneous nucleation of the newly formed Pd atoms. The small particles generated in the growth phase could be consumed with the assistance of Ostwald ripening.³⁸ However, the process was extremely slow and typically took about 48 h to complete because of the low concentration of larger particles.

Here, we report a robust route to the synthesis of Pd icosahedral nanocrystals with uniform and controllable sizes by combining polyol reduction with seed-mediated growth. Our mechanistic study demonstrates that Ostwald ripening plays a vital role in the synthesis, by which the size distribution of the particles is narrowed within a short period of time due to the "size focusing" effect. By simply terminating the synthesis at different time points, Pd icosahedral nanocrystals with uniform and controllable sizes in the range of 6.8–10.7 nm can be

obtained using a standard protocol. The size can be further extended up to 19.2 nm without compromising the quality via seed-mediated growth, with the uniform particles synthesized through Ostwald ripening serving as the seeds. In this case, the slow reduction kinetics of $PdBr_4^{2-}$ ensures surface reduction and, thus, layer-by-layer growth of Pd icosahedral nanocrystals into enlarged sizes, whereas the fast kinetics of $PdCl_4^{2-}$ also allows for direct reduction in the solution phase, resulting in homogeneous nucleation. As a result, Pd icosahedral nanocrystals with uniform and predictable sizes up to 20 nm can be obtained through one-shot injection of different amounts of $PdBr_4^{2-}$ into the growth solution.

■ RESULTS AND DISCUSSION

Ostwald Ripening and the "Size Focusing" Effect. We synthesized Pd icosahedral nanocrystals using a polyol method based on diethylene glycol (DEG). A typical synthesis involved the one-shot injection of Na₂PdCl₄ (dissolved in DEG) into another DEG solution containing poly-(vinylpyrrolidone) (PVP) at 130 °C. In this protocol, Na₂PdCl₄ and PVP served as a precursor to elemental Pd and a colloidal stabilizer, respectively, while DEG acted as a solvent and a precursor to the reductant. Within 10 min, the color of the reaction solution changed from light reddish-brown to deep black, indicating the formation of Pd nanocrystals. After about 3 h, the nanocrystals did not grow in size anymore and could be collected by centrifugation.

Figure 1a shows a typical TEM image of the Pd icosahedral nanocrystals obtained using the standard protocol. At a relatively low magnification, this image demonstrates nearly 98% purity in terms of icosahedral shape. Only a very small fraction of the particles took the decahedral or cuboctahedral (i.e., the single-crystal structure) shape (Figure 1b). 26,28 The particles showed a narrow distribution in size, with an average size of 10.7 ± 0.4 nm. In this paper, the "size" of an icosahedron refers to the dimension "l" defined in Figure S1, which corresponds to the distance between two opposite side faces. In general, icosahedral nanocrystals can exhibit different profiles under TEM depending on their orientations relative to the electron beam. Three of them are most popular, with the electron beam aligned along the 2-, 3- and 5-fold axes, respectively. The atomic-resolution HAADF-STEM image in Figure 1c shows an individual Pd icosahedral nanocrystal oriented with its 2-fold axis parallel to the electron beam. The corresponding model can be found in the inset. The HAADF-STEM images of other Pd icosahedral nanocrystals situated along the 3- and 5-fold axes can be found in Figure S2. Figure 1d shows a X-ray diffraction pattern of the sample, which identifies high crystallinity and phase purity of the as-prepared Pd icosahedral nanocrystals. All the diffraction peaks can be indexed to fcc Pd (JCPDS card 05-0681). The intensity ratio of the (111) peak to the (200) peak is greater than the value of the conventional powder sample (2.8 versus 2.4), implying that the diffraction from {111} planes was enhanced for the icosahedral nanocrystals due to the texturing effect. Moreover, several of the diffraction peaks are clearly split, different from those of Pd powders recorded in JCPDS. This could be attributed to the high density of twin defects and, thus, the induced strain that can alter the lattice spacing.³⁸ Using the Scherrer equation, the mean size of the Pd icosahedral nanocrystals derived from the (111) peak was only 4.4 nm. The discrepancy between the particle sizes derived from XRD analysis and TEM imaging can also be attributed to the high

density of twin boundaries contained in the icosahedral nanocrystals.

We investigated the morphological evolution of the Pd nanocrystals by taking samples at different stages of a standard synthesis and analyzing them by TEM. Figure 2a–d shows

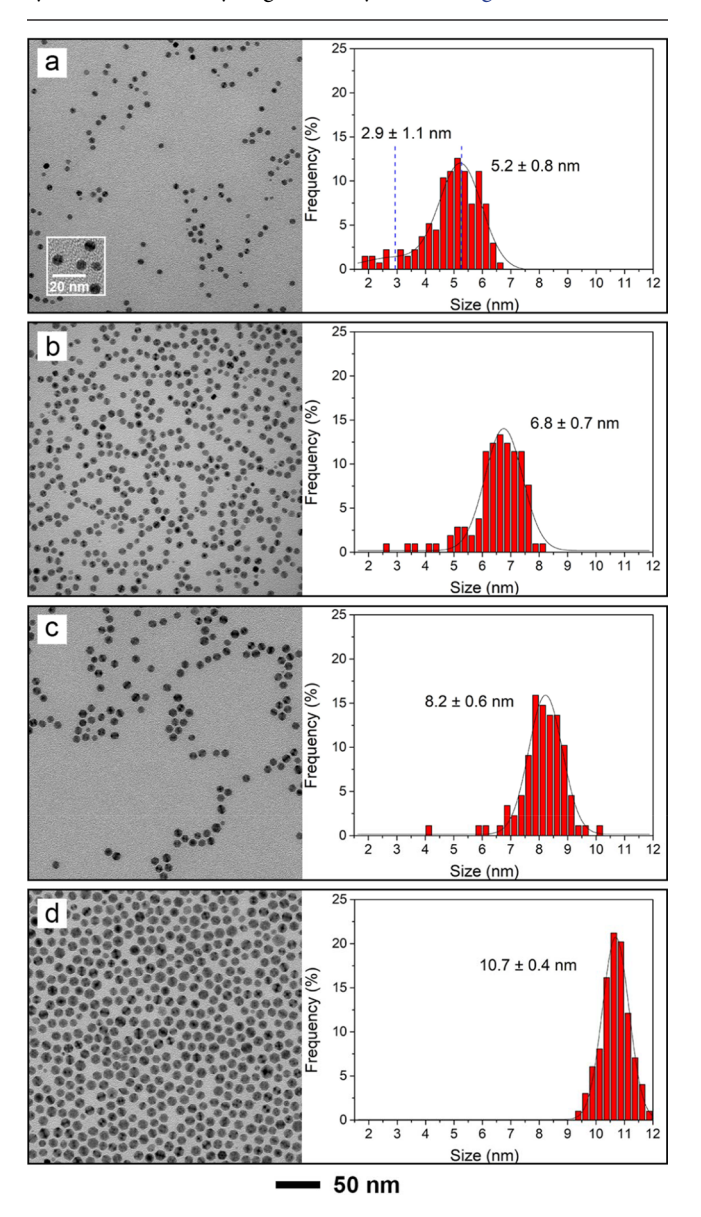


Figure 2. TEM images and size distributions of the samples obtained using the same standard protocol except for the variation in reaction time: (a) 10, (b) 30, (c) 60, and (d) 180 min. The scale bar at the bottom applies to all panels, with the inset in (a) showing the particles at an enlarged magnification.

TEM images and size distributions of the products sampled at t=10, 30, 60, and 180 min, respectively. At t=10 min, the sample mainly contained small particles with a nearly circular profile (Figure 2a). The size of the particles exhibited a bimodal distribution. The population at the smaller size corresponded to the just-formed nuclei/seeds, whose internal structure could not be resolved from the TEM image. In contrast, the population at the larger size showed a multiply-twined structure, together with an average size of 5.2 nm (Figure 2a). At t=30 min, particles with an icosahedral shape were observed, as indicated by the characteristic hexagonal

profile under TEM. Most of the nuclei/seeds had disappeared at this point, while the multiply twined particles had grown to an average size of 6.8 nm. Accordingly, the bimodal size distribution observed at the earlier stage changed into a unimodal distribution (Figure 2b). When the reaction time was extended to 60 and 180 min, nearly all the small nuclei/seeds had disappeared, while the icosahedral nanocrystals further grew to average sizes of 8.2 and 10.7 nm, respectively. The size distribution of the particles was also narrowed with reaction time, as reflected by the decrease in standard deviation (Figure 3). It is worth pointing out that the standard deviation at t = 10

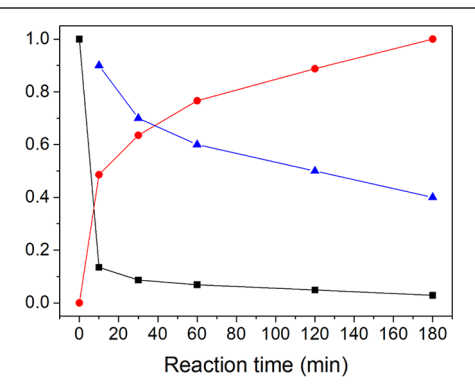


Figure 3. Red trace: particle size (normalized to the final size obtained at t=180 min) as a function of reaction time. Black trace: concentration of Pd(II) precursor in the reaction solution (normalized to the initial concentration) as a function of reaction time. Blue trace: standard deviation of the particle sizes (unit: nm) as a function of reaction time. Note that the particle size still increased by more than 50% beyond t=10 min while the concentration of Pd(II) remained essentially the same, implying the dominant role played by Ostwald ripening in enlarging the particle size.

min was calculated for all the particles, including the nuclei/seeds, in the sample, thus differing from the separately calculated values shown in Figure 2a. These results suggest the involvement of Ostwald ripening in the growth process, by which the larger icosahedral nanocrystals grew at the expenses of the smaller nuclei/seeds.

Atomic addition (ripening-mediated or precursor-enabled) and aggregative process can both contribute to the growth of colloidal metal nanocrystals.⁴⁰ In the present synthesis, the aggregation-based growth mechanism can be excluded as no coalescence intermediates (e.g., dumbbell-shaped particles) was observed in the TEM images.⁴¹ As such, the growth mechanisms can be narrowed down to ripening-mediated or precursor-enabled growth. The difference between these two mechanisms mainly comes from the source of new Pd atoms being incorporated into the growing icosahedral nanocrystals. In the latter case, the growth of Pd icosahedral nanocrystals is accompanied by a decrease in the concentration of Pd(II) precursor. As for Ostwald ripening, the concentration of Pd(II) precursor should remain the same during the growth. To differentiate these two mechanisms, we used inductively coupled plasma mass spectrometry (ICP-MS) to measure the concentrations of Pd(II) in the reaction solution at the same time points used for studying size evolution by TEM. Figure 3 compares the changes to the concentration of Pd(II) species and the corresponding increases in particle size as a function of reaction time. Almost all the Pd(II) precursor had been consumed within 10 min into the synthesis, while the icosahedral nanocrystals could still grow and be significantly

enlarged even after t=10 min. This result confirms the dominant role played by Ostwald ripening rather than precursor reduction in the growth process.

Our mechanistic study demonstrates that the "size focusing" effect of Ostwald ripening also plays a pivotal role in the colloidal synthesis of metal nanocrystals as a uniform sample. Since the polyol synthesis is conducted at a relatively high temperature and under an ambient atmosphere, Ostwald ripening can be easily initiated and maintained through the involvement of oxidative etching. As demonstrated above, the broad distribution in size for the initial particles could be quickly narrowed through Ostwald ripening, resulting in Pd icosahedral nanocrystals with uniform sizes controllable in the range of 6.8-10.7 nm. Within this range, the size of the Pd icosahedral nanocrystals could be conveniently tuned by terminating the synthesis at different time points because the particles followed a layer-by-layer growth mode. It is anticipated that Ostwald ripening and its "size-focusing effect" observed in the growth of Pd icosahedral nanocrystals can be extended to other systems involving metal nanocrystals with different compositions, shapes, facets, and internal structures. However, it should be emphasized that the thermodynamical driving force for Oswald ripening will eventually disappear when the size distribution is narrowed to reach an equilibrium state. In the standard synthesis of Pd icosahedral nanocrystals, the size enlargement would essentially stop after the growth had processed for about 3 h. As a result, this growth mechanism can only be utilized to tune the size of the particles within a limited range. It was reported that Pd icosahedral nanocrystals with sizes larger than 11 nm could be synthesized using a similar method.³⁸ The initial reduction rate of the metal precursor, PdCl₄²⁻, was lowered to reduce the number of seeds formed in the nucleation stage. Accordingly, the size of the final product was increased when the amount of metal precursor was fixed. However, a large number of small particles would also form during the growth phase due to the involvement of solution reduction of PdCl₄²⁻ and additional homogeneous nucleation of the newly formed Pd atoms. Although these small particles could be consumed with the help of Ostwald ripening, the process was extremely slow because of the low concentration of larger particles. According to those authors, the synthesis typically took about 48 h to complete. Therefore, to quickly access Pd icosahedral nanocrystals with average sizes beyond 11 nm, one has to rely on other methods such as seed-mediated growth.

Size Enlargement via Seed-Mediated Growth. Nanocrystals that are uniform in size are highly desired for the reliable investigation of their properties. As shown in the last section, the growth based on Ostwald ripening can only be used to tune the size of Pd icosahedral nanocrystals in a relatively narrow range of 6.8–10.7 nm. However, a systematic study of the properties as a function of particle size would require samples with uniform sizes over a broader range.

Seed-mediated growth is probably the most effective strategy for enlarging the size of colloidal particles. Using the preformed Pd icosahedral nanocrystals as seeds, particles with enlarged sizes can be obtained through layer-by-layer growth under appropriate conditions. In general, the facets expressed on the final nanocrystals could be kept the same as those on the seed. For the Pd icosahedral nanocrystal, its surface is exclusively enclosed by {111} facets. Unless there is a capping agent to preferentially stabilize {100} or {110} facets, {111} facets should be the lowest in surface energy among all

the facets commonly exposed on nanocrystals made of an fcc metal. As such, there is no need to stabilize and preserve the {111} facets by introducing a specific capping agent. When the icosahedral nanocrystal is stellated, each {111} side face would become convex and covered by three {100} facets (Figure S3). This will result in a higher surface energy because of a larger surface to volume ratio and the creation of {100} facets greater in energy than {111} facets. As a result, layer-by-layer growth should be more favorable as it helps preserve {111} facets on the side faces.

The Pd atoms to be deposited can be derived from a newly added precursor such as $PdCl_4^{\ 2^-}$ or $PdBr_4^{\ 2^-}$. After the completion of a standard synthesis, the precursor can be directly introduced into the reaction solution without separating out the preformed seeds. To avoid homogeneous nucleation and related complications, the reduction kinetics should be carefully controlled. In the first attempt, we titrated additional $PdCl_4^{\ 2^-}$ (dissolved in DEG) dropwise into the reaction solution held at 130 °C using a syringe pump. The syringe pump was used to tightly regulate the injection rate of $PdCl_4^{\ 2^-}$ and thus maintain the instantaneous concentration of $PdCl_4^{\ 2^-}$ at a low level throughout the growth process. Figure 4

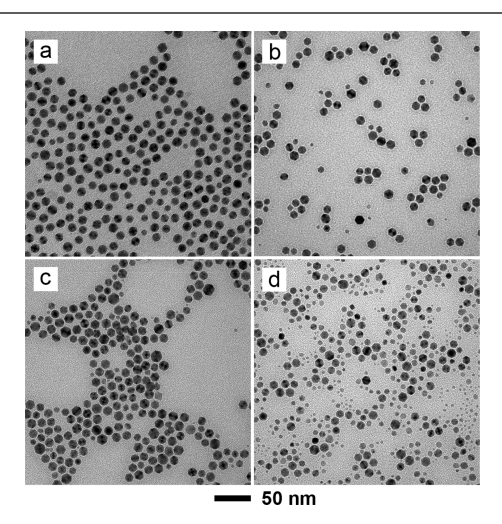


Figure 4. TEM images of the samples obtained by adding different volumes of $\mathrm{Na_2PdCl_4}$ solution (dissolved in DEG, 0.065 mg/mL) into the reaction solution corresponding to the sample shown in Figure 2d: (a) 0.5, (b) 1.5, (c) 5, and (d) 20 mL, respectively, at an injection rate of 1 mL/h. Note the formation of additional smaller particles due to the involvement of solution reduction and, thus, homogeneous nucleation for the newly formed Pd atoms.

shows TEM images of the as-obtained products. Even after a small amount of $PdCl_4^{\ 2^-}$ had been introduced, a new population of smaller particles was formed (Figure 4b), indicating that the newly formed Pd atoms went through homogeneous nucleation upon the reduction of $PdCl_4^{\ 2^-}$. Although the concentration of $PdCl_4^{\ 2^-}$ was kept at a very low level, its reduction rate was fast enough to induce solution reduction. As $PdCl_4^{\ 2^-}$ was continuously introduced into the reaction solution, more small particles were formed, resulting in products plagued by poor purity and uniformity (Figure 4d). The products obtained by injecting $PdCl_4^{\ 2^-}$ (also dissolved in DEG) in one shot are shown in Figure S4. Similarly, smaller particles were also formed due to the involvement of solution reduction and, thus, homogenous nucleation.

The broad size distribution of the particles and the increase in size for the Pd icosahedral nanocrystals suggest that Ostwald ripening might also be involved in this seed-mediated growth process (Figure 4a-d). The small particles generated through homogenous nucleation could be dissolved into DEG and then redeposited onto the existing icosahedral nanocrystals via Ostwald ripening, providing another route to enlarge the size of the particles. However, the small particles failed to dissolve within the short period of time we used as a result of the slowness of a typical Ostwald ripening process. At the end of a standard synthesis of Pd icosahedral nanocrystals, the concentration of particles should be the lowest, resulting in the greatest interparticle distance. As such, it would take a long time for the dissolved species to diffuse from small particles to larger ones.

Our previous quantitative analysis of the kinetics suggests that the reduction pathway of a precursor can be switched from solution reduction to surface reduction by decreasing the reduction rate. Therefore, we replaced $PdCl_4^{2-}$ with $PdBr_4^{2-}$, a complex known for its relatively slow reduction kinetics. Immediately after a standard synthesis of Pd icosahedral nanocrystals, $PdBr_4^{2-}$ (dissolved in DEG) was injected into the reaction mixture in one shot using a pipette. As shown in Figure 5, the size of the resultant Pd icosahedral nanocrystals

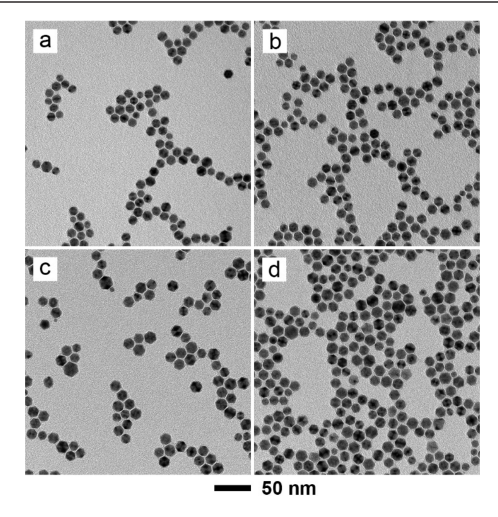


Figure 5. TEM images of the samples obtained by adding (in one shot) 0.4 mL of K_2PdBr_4 solution (dissolved in DEG, 15 mg/mL) into the reaction solution corresponding to the sample shown in Figure 2d and waiting for different periods of time: (a) 15, (b) 60, (c) 120, and (d) 180 min. Note the absence of a new population of smaller particles due to the dominance of surface reduction and, thus, elimination of homogeneous nucleation. The size of the icosahedral nanocrystals increased from 10.7 to 14.3 nm as a result of surface reduction and layer-by-layer growth.

increased with time, while the icosahedral morphology was well maintained during the growth process. The characteristic twin contrasts could still be resolved in the TEM images. These results indicated that the slow reduction rate of $PdBr_4^{2-}$ led to layer-by-layer deposition of the newly formed Pd atoms on the surface of existing particles. Because of layer-by-layer growth, the size of the Pd icosahedral nanocrystals could be precisely tuned by controlling the amount of the added $PdBr_4^{2-}$ precursor. In most cases of seed-mediated growth, experimental parameters must be carefully optimized to ensure layer-by-layer deposition on the seeds. The solution containing

metal precursor is often titrated into the growth solution dropwise with the assistance of a syringe pump in order to keep the concentration of newly formed atoms below a certain level and thus avoid homogenous nucleation. Trial-and-error experiments are usually conducted to coordinate different experimental parameters such as the injection rate of precursor and reaction temperature. In the present case, since the PdBr₄²⁻ precursor has a favorable slow kinetics for surface reduction, it can be added into the growth solution in one shot without performing any trial-and-error experiments to optimize the experimental parameters. As shown in Figure 5c,d, in the case of one-shot injection of PdBr₄²⁻, the Pd icosahedral nanocrystals nearly stopped growing 120 min after the precursor solution had been introduced.

The size of the Pd icosahedral nanocrystals could be further enlarged by varying the amount of PdBr₄²⁻ added into the reaction solution. Using this approach, the average size of the Pd icosahedral nanocrystals could be increased up to 19.2 nm (Figure 6). At this point, the Pd icosahedral nanocrystals

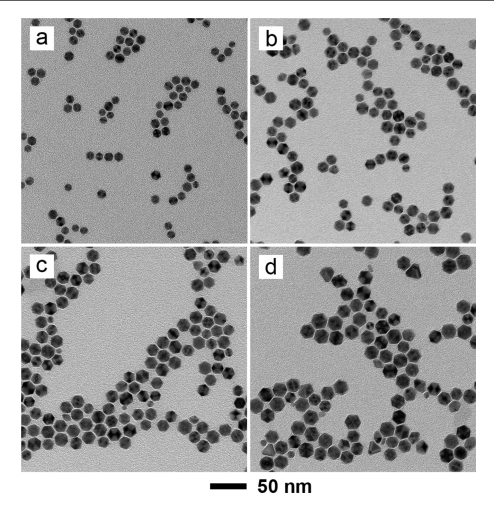


Figure 6. TEM images of the samples obtained by adding (in one shot) different volumes of K_2PdBr_4 solution (dissolved in DEG, 15 mg/mL) into the reaction solution corresponding to the sample shown in Figure 2d: (a) 0.2, (b) 1.5, (c) 5, and (d) 12 mL, respectively.

stopped growing or grew at an extremely slow rate, together with the accumulation of PdBr₄²⁻ in the reaction solution to a high concentration. A different population of smaller particles was observed, indicating the occurrence of solution reduction and homogeneous nucleation (Figure 6d). This result suggests that metal atoms prefer to undergo homogenous nucleation rather than be deposited onto the existing particles. The upper limit on the size of the Pd icosahedral nanocrystals obtained using the seed-mediated growth can be understood from different perspectives. First, according to the trend derived from theoretical calculations, as the size increases, the energetic contribution from twin defects contained in an icosahedral particle and the consequent tensile strain distributed on the surface would increase drastically. 21 As a result, the icosahedral structure would become energetically unfavorable when the size reaches a certain value (i.e., 20 nm in the present case) because the reduction in bulk energy resulting from bond formation can no longer compensate the increase in surface free energy caused by the twin defect and consequent tensile strain.²³ The largest size reported for Pd icosahedral

nanocrystals was about 42 nm.38 In that synthesis, PdCl₄2was used as a precursor in the growth phase instead of PdBr₄² As mentioned earlier, additional small particles were also formed in the growth phase due to the involvement of solution reduction of $PdCl_4^{2-}$ and homogeneous nucleation of the newly formed Pd atoms, which could then contribute to growth via Ostwald ripening. The driving force for Ostwald ripening could eventually overcome the upper size limit of the Pd icosahedral nanocrystals (i.e., 20 nm) observed in our work.⁴³ Second, oxidative etching of twin defects might also affect the upper size limit of the Pd icosahedral nanocrystals. As the particle size is enlarged, the enhanced tensile strain and enlarged twin boundaries on the surface will make the icosahedral nanocrystals more susceptible to oxidative etching. 44 When the size of icosahedral nanocrystals reached 20 nm, they could be readily etched by the O₂/Br⁻ pair, transforming them into decahedral and tetrahedral nanocrystals (Figure S7). It is unlikely that the Pd icosahedral nanocrystals physically transformed to decahedral and tetrahedral nanocrystals because a high thermal energy would be required to overcome atom diffusion barriers during such a transition and it could not be achieved under our experimental conditions. This also explains why the size of the Pd icosahedral nanocrystals could be increased beyond 20 nm in in literature.³⁸ Their synthesis only involved Cl⁻, a coordination ligand known for its weaker etching power than Br⁻.45

The maximum particle size in our system can potentially be increased by adding citric acid into the reaction solution. On one hand, citric acid binds strongly to $\{111\}$ facets, helping compensate for the extra free energy caused by twin defect and tensile strain by reducing the surface energy. On the other hand, citric acid can help scavenger oxygen from the solution or compete with O_2 adsorption on the $\{111\}$ facets, thereby suppressing oxidative etching.

It is worth noting that it is supposed to be much easier to obtain large Au and Ag icosahedral nanocrystals due to the relatively low twin-defect energy of Au (26 mJ m⁻²) and Ag (16 mJ m⁻²) as compared to that of Pd (106 mJ m⁻²). Moreover, the dissolved oxygen binds less strongly to Ag or Au than to Pd, greatly reducing the rate of the oxidative etching relative to that of the Pd nanocrystals.⁹

CONCLUSIONS

In summary, we have systematically investigated a DEG-based polyol method for the robust synthesis of Pd icosahedral nanocrystals with uniform and tunable sizes up to 20 nm. By following the concentration of Pd(II) in the reaction solution and the particle size, we validated the critical role played by Ostwald ripening in generating a uniform sample. Due to the "size focusing" effect enabled by Ostwald ripening, the particles initially formed through homogenous nucleation were quickly narrowed in size for the synthesis of Pd icosahedral nanocrystals with uniform sizes controllable up to 11 nm simply by stopping the reaction at different time points. To further enlarge the particles, seed-mediated growth has been utilized, with the uniform Pd icosahedral nanocrystals synthesized via Ostwald ripening serving as the seeds. In this step, it was vital to prevent homogeneous nucleation by choosing an appropriate precursor to slow down the reduction kinetics and thus favor surface reduction. Specifically, by directly injecting PdBr₄²⁻ into the reaction solution in one shot, the seeds could grow in a layer-by-layer fashion to obtain

enlarged particles, with the final size mainly determined by the amount of the newly added precursor. We believe that the mechanistic understanding and experimental controls demonstrated in this work can be extended to other systems, offering insightful guidance for the rational synthesis of noble-metal nanocrystals with well-controlled compositions, sizes, shapes, and internal structures.

■ EXPERIMENTAL SECTION

Chemicals and Materials. Diethylene glycol (DEG, 99.0%, lot no. BCBJ9740), sodium tetrachloropalladate(II) (Na₂PdCl₄, 99.998%), potassium tetrabromopalladate(II) (K₂PdBr₄, 99.998%), and poly(vinyl pyrrolidone) (PVP, $M_{\rm w} \approx 55,\!000$) were all obtained from Sigma-Aldrich and used as received. Deionized (DI) water with a resistivity of 18.2 M Ω cm at room temperature was used throughout the experiments.

Characterizations. All transmission electron microscopy (TEM) images were captured using a Hitachi HT7700 microscope. The sample was prepared by adding a drop of the aqueous suspension onto a carbon-coated Cu grid and then allowing it to dry under ambient conditions. The high-resolution scanning transmission electron microscopy (STEM) images were captured using a Hitachi HD 2700 with an acceleration voltage of 200 kV. The concentration of the Pd(II) precursor remaining in the reaction solution was determined using inductively coupled plasma mass spectrometry (ICP-MS, PerkinElmer, NexION 300Q). The sample was prepared by dissolving the particles in aqua regia and further diluted with 1% (vol/vol) aqueous HNO₃ solution to a level of 100 ppb. X-ray diffraction (XRD) patterns were obtained on Panalytical XPert PRO Alpha-1 with Cu K_a, radiation.

Synthesis of the Pd lcosahedral Nanocrystals. The nanocrystals with an average size of 10 nm were synthesized according to our previously reported protocol. In a standard process, 80 mg of PVP was dissolved in 2 mL of DEG hosted in a 20 mL vial by heating at 130 °C for 10 min under magnetic stirring. Meanwhile, 15.5 mg of Na₂PdCl₄ was dissolved in 1 mL of DEG, and the solution was then injected into the PVP solution in one shot. The reaction was maintained at 130 °C for 3 h under magnetic stirring. The solid products were crushed out using 20 mL of acetone, collected by centrifugation, and washed once with acetone and twice with ethanol. Finally, the Pd icosahedral nanocrystals were redispersed in 1 mL of water for further characterization.

Seed-Mediated Growth of the Pd Icosahedral Nanocrystals. To enlarge the size of the Pd icosahedral nanocrystals, PdCl₄²⁻ or PdBr₄²⁻ (dissolved in DEG) was added into the reaction solution when the Pd icosahedral nanocrystals stopped growing (after 3 h into a standard synthesis). In the first set of experiments, a Na₂PdCl₄ solution in DEG (0.065 mg/mL) was titrated into the 20 mL vial containing 1 mL of the reaction solution at a rate of 1 mL/h. Samples were collected after the addition of 0.5, 1.5, 5, and 20 mL of the Na₂PdCl₄ solution for TEM measurements (Figure 4). For comparison, another Na₂PdCl₄ solution (0.4 mL, 8.75 mg/mL) was also injected in one shot into another 20 mL vial containing 1 mL of the reaction solution. In this case, samples were collected after different periods of time: 15, 60, 120, and 180 min (Figure S4). In the second set of experiments, a K₂PdBr₄ solution in DEG (0.4 mL, 15 mg/mL) was added in one shot into 1 mL of the reaction solution. Samples were collected after different periods of time: 15, 60, 120, and 180 min (Figure 5). For comparison, different volumes (0.2, 1.5, 5, and 12 mL) of the same K₂PdBr₄ solution in DEG (15 mg/mL) were added into 1 mL of the reaction solution, respectively, and samples were collected after 120 min into the growth (Figure 6). After each synthesis, the solid products were crushed out using 20 mL of acetone, collected by centrifugation, and washed once with acetone and twice with ethanol. Finally, the particles were redispersed in 1 mL of water for further characterization.

ASSOCIATED CONTENT

Solution Supporting Information

The Supporting Information is available free of charge at https://pubs.acs.org/doi/10.1021/acs.chemmater.2c00397.

Schematic showing how the particle size (l) is defined for a Pd icosahedral nanocrystal; HAADF-STEM images of Pd icosahedral nanocrystals oriented along the 3- and 5-fold axes; Schematic showing a model of a stellated icosahedron enclosed by {100} facets; TEM images of the products obtained by adding PdCl₄ $^{2-}$ solution in one shot; TEM images and size distributions of the Pd icosahedral nanocrystals prepared by adding PdBr₄ $^{2-}$ solution in one shot (PDF)

AUTHOR INFORMATION

Corresponding Author

Younan Xia — School of Chemical and Biomolecular Engineering and School of Chemistry and Biochemistry, Georgia Institute of Technology, Atlanta, Georgia 30332, United States; The Wallace H. Coulter Department of Biomedical Engineering, Georgia Institute of Technology and Emory University, Atlanta, Georgia 30332, United States; orcid.org/0000-0003-2431-7048; Email: younan.xia@bme.gatech.edu

Authors

Siyu Zhou — School of Chemical and Biomolecular Engineering, Georgia Institute of Technology, Atlanta, Georgia 30332, United States; orcid.org/0000-0001-5959-0541

Chenxiao Wang — School of Chemistry and Biochemistry, Georgia Institute of Technology, Atlanta, Georgia 30332, United States

Complete contact information is available at: https://pubs.acs.org/10.1021/acs.chemmater.2c00397

Notes

The authors declare no competing financial interest.

ACKNOWLEDGMENTS

This work was supported in part by two grants from NSF (CHE 1804970 and 2105602) and start-up funds from the Georgia Institute of Technology. TEM and STEM imaging was performed at the Georgia Tech Institute for Electronics and Nanotechnology, a member of the National Nanotechnology Coordinated Infrastructure (NNCI), which is supported by the National Science Foundation (ECCS-2025462).

REFERENCES

- (1) Shi, Y.; Lyu, Z.; Zhao, M.; Chen, R.; Nguyen, Q. N.; Xia, Y. Noble-Metal Nanocrystals with Controlled Shapes for Catalytic and Electrocatalytic Applications. *Chem. Rev.* **2021**, *121*, 649–735.
- (2) Liu, L.; Corma, A. Metal Catalysts for Heterogeneous Catalysis: From Single Atoms to Nanoclusters and Nanoparticles. *Chem. Rev.* **2018**, *118*, 4981–5079.
- (3) Dreaden, E. C.; Alkilany, A. M.; Huang, X.; Murphy, C. J.; El-Sayed, M. A. The golden age: gold nanoparticles for biomedicine. *Chem. Soc. Rev.* **2012**, *41*, 2740–2779.
- (4) Fafarman, A. T.; Hong, S. H.; Oh, S. J.; Caglayan, H.; Ye, X.; Diroll, B. T.; Engheta, N.; Murray, C. B.; Kagan, C. R. Air-stable, nanostructured electronic and plasmonic materials from solution-processable, silver nanocrystal building blocks. *ACS Nano* **2014**, *8*, 2746–2754.

- (5) Choi, J. H.; Wang, H.; Oh, S. J.; Paik, T.; Sung, P.; Sung, J.; Ye, X.; Zhao, T.; Diroll, B. T.; Murray, C. B.; Kagan, C. R. Exploiting the colloidal nanocrystal library to construct electronic devices. *Science* **2016**, 352, 205–208.
- (6) Henzie, J.; Andrews, S. C.; Ling, X. Y.; Li, Z.; Yang, P. Oriented assembly of polyhedral plasmonic nanoparticle clusters. *Proc. Natl. Acad. Sci. U. S. A.* **2013**, *110*, 6640–6645.
- (7) Zhang, Y.; Ahn, J.; Liu, J.; Qin, D. Syntheses, Plasmonic Properties, and Catalytic Applications of Ag—Rh Core-Frame Nanocubes and Rh Nanoboxes with Highly Porous Walls. *Chem. Mater.* **2018**, *30*, 2151–2159.
- (8) Liu, N.; Tang, M. L.; Hentschel, M.; Giessen, H.; Alivisatos, A. P. Nanoantenna-enhanced gas sensing in a single tailored nanofocus. *Nat. Mater.* **2011**, *10*, 631–636.
- (9) Wang, H.; Zhou, S.; Gilroy, K. D.; Cai, Z.; Xia, Y. Icosahedral nanocrystals of noble metals: Synthesis and applications. *Nano Today* **2017**, *15*, 121–144.
- (10) Wang, X.; Choi, S. I.; Roling, L. T.; Luo, M.; Ma, C.; Zhang, L.; Chi, M.; Liu, J.; Xie, Z.; Herron, J. A.; Mavrikakis, M.; Xia, Y. Palladium-platinum core-shell icosahedra with substantially enhanced activity and durability towards oxygen reduction. *Nat. Commun.* **2015**, *6*, 7594.
- (11) Wang, X.; Figueroa-Cosme, L.; Yang, X.; Luo, M.; Liu, J.; Xie, Z.; Xia, Y. Pt-Based Icosahedral Nanocages: Using a Combination of {111} Facets, Twin Defects, and Ultrathin Walls to Greatly Enhance Their Activity toward Oxygen Reduction. *Nano Lett.* **2016**, *16*, 1467–1471.
- (12) Liu, M.; Lyu, Z.; Zhang, Y.; Chen, R.; Xie, M.; Xia, Y. Twin-Directed Deposition of Pt on Pd Icosahedral Nanocrystals for Catalysts with Enhanced Activity and Durability toward Oxygen Reduction. *Nano Lett.* **2021**, 21, 2248–2254.
- (13) Wu, J.; Qi, L.; You, H.; Gross, A.; Li, J.; Yang, H. Icosahedral platinum alloy nanocrystals with enhanced electrocatalytic activities. *J. Am. Chem. Soc.* **2012**, *134*, 11880–11883.
- (14) Wang, Y.; Zheng, Y.; Huang, C. Z.; Xia, Y. Synthesis of Ag nanocubes 18-32 nm in edge length: The effects of polyol on reduction kinetics, size control, and reproducibility. *J. Am. Chem. Soc.* **2013**, *135*, 1941–1951.
- (15) Zhao, M.; Holder, J.; Chen, Z.; Xie, M.; Cao, Z.; Chi, M.; Xia, Y. Facile Synthesis of Pt Icosahedral Nanocrystals with Controllable Sizes for the Evaluation of Size-Dependent Activity toward Oxygen Reduction. *ChemCatChem* **2019**, *11*, 2458–2463.
- (16) Wang, H.; Gu, X. K.; Zheng, X.; Pan, H.; Zhu, J.; Chen, S.; Cao, L.; Li, W. X.; Lu, J. Disentangling the size-dependent geometric and electronic effects of palladium nanocatalysts beyond selectivity. *Sci. Adv.* 2019, 5, No. eaat6413.
- (17) Cao, S.; Tao, F. F.; Tang, Y.; Li, Y.; Yu, J. Size- and shape-dependent catalytic performances of oxidation and reduction reactions on nanocatalysts. *Chem. Soc. Rev.* **2016**, *45*, 4747–4765.
- (18) Reske, R.; Mistry, H.; Behafarid, F.; Roldan Cuenya, B.; Strasser, P. Particle size effects in the catalytic electroreduction of CO₂ on Cu nanoparticles. *J. Am. Chem. Soc.* **2014**, *136*, 6978–6986.
- (19) Den Breejen, J. P.; Radstake, P. B.; Bezemer, G. L.; Bitter, J. H.; Frøseth, V.; Holmen, A.; de Jong, K. P. On the origin of the cobalt particle size effects in Fischer-Tropsch catalysis. *J. Am. Chem. Soc.* **2009**, *131*, 7197–7203.
- (20) Kuhn, J. N.; Huang, W.; Tsung, C. K.; Zhang, Y.; Somorjai, G. A. Structure sensitivity of carbon-nitrogen ring opening: impact of platinum particle size from below 1 to 5 nm upon pyrrole hydrogenation product selectivity over monodisperse platinum nanoparticles loaded onto mesoporous silica. *J. Am. Chem. Soc.* **2008**, *130*, 14026–14027.
- (21) Barnard, A. S.; Young, N. P.; Kirkland, A. I.; Van Huis, M. A.; Xu, H. Nanogold: A quantitative phase map. *ACS Nano* **2009**, 3, 1431–1436.
- (22) González, A. L.; Noguez, C.; Barnard, A. S. Map of the structural and optical properties of gold nanoparticles at thermal equilibrium. *J. Phys. Chem. C* 2012, *116*, 14170–14175.

- (23) Gilroy, K. D.; Puibasset, J.; Vara, M.; Xia, Y. On the Thermodynamics and Experimental Control of Twinning in Metal Nanocrystals. *Angew. Chem., Int. Ed.* **2017**, *56*, 8647–8651.
- (24) Favier, I.; Pla, D.; Gómez, M. Palladium Nanoparticles in Polyols: Synthesis, Catalytic Couplings, and Hydrogenations. *Chem. Rev.* **2020**, *120*, 1146–1183.
- (25) Ruditskiy, A.; Vara, M.; Huang, H.; Xia, Y. Oxidative Etching of Pd Decahedral Nanocrystals with a Penta-twinned Structure and Its Impact on Their Growth Behavior. *Chem. Mater.* **2017**, *29*, 5394–5400
- (26) Wang, Y.; Peng, H. C.; Liu, J.; Huang, C. Z.; Xia, Y. Use of reduction rate as a quantitative knob for controlling the twin structure and shape of palladium nanocrystals. *Nano Lett.* **2015**, *15*, 1445–1450.
- (27) Lv, T.; Wang, Y.; Choi, S. I.; Chi, M.; Tao, J.; Pan, L.; Huang, C. Z.; Zhu, Y.; Xia, Y. Controlled synthesis of nanosized palladium icosahedra and their catalytic activity towards formic-acid oxidation. *ChemSusChem* **2013**, *6*, 1923–1930.
- (28) Huang, H.; Wang, Y.; Ruditskiy, A.; Peng, H. C.; Zhao, X.; Zhang, L.; Liu, J.; Ye, Z.; Xia, Y. Polyol syntheses of palladium decahedra and icosahedra as pure samples by maneuvering the reaction kinetics with additives. *ACS Nano* **2014**, *8*, 7041–7050.
- (29) Wang, W.; Zhou, S.; Shen, M.; Hood, Z. D.; Xiao, K.; Xia, Y. Facile Synthesis of Silver Icosahedral Nanocrystals with Uniform and Controllable Sizes. *ChemNanoMat* **2018**, *4*, 1071–1077.
- (30) Chen, L.; Leong, G. J.; Schulze, M.; Dinh, H. N.; Pivovar, B.; Hu, J.; Qi, Z.; Fang, Y.; Prikhodko, S.; Pozuelo, M.; Kodambaka, S.; Richards, R. M. Controlled Synthesis of Nanoscale Icosahedral Gold Particles at Room Temperature. *ChemCatChem* **2012**, *4*, 1662–1667.
- (31) Lim, B.; Xiong, Y.; Xia, Y. A water-based synthesis of octahedral, decahedral, and icosahedral Pd nanocrystals. *Angew. Chem., Int. Ed. Engl.* **2007**, *46*, 9279–9282.
- (32) LaMer, V. K.; Dinegar, R. H. Theory, Production and Mechanism of Formation of Monodispersed Hydrosols. *J. Am. Chem. Soc.* **1950**, 72, 4847–4854.
- (33) Johnson, N. J. J.; Korinek, A.; Dong, C.; van Veggel, F. C. J. M. Self-focusing by Ostwald ripening: a strategy for layer-by-layer epitaxial growth on upconverting nanocrystals. *J. Am. Chem. Soc.* **2012**, *134*, 11068–11071.
- (34) Talapin, D. V.; Rogach, A. L.; Haase, M.; Weller, H. Evolution of an Ensemble of Nanoparticles in a Colloidal Solution: Theoretical Study. *J. Phys. Chem. B* **2001**, *105*, 12278–12285.
- (35) Chen, Y.; Johnson, E.; Peng, X. Formation of monodisperse and shape-controlled MnO nanocrystals in non-injection synthesis: self-focusing via ripening. *J. Am. Chem. Soc.* **2007**, *129*, 10937–10947.
- (36) Dai, Y.; Lu, P.; Cao, Z.; Campbell, C. T.; Xia, Y. The Physical Chemistry and Materials Science behind Sinter-Resistant Catalysts. *Chem. Soc. Rev.* **2018**, *47*, 4314–4331.
- (37) Zhang, C.; Xia, Y.; Zhang, Z.; Huang, Z.; Lian, L.; Miao, X.; Zhang, D.; Beard, M. C.; Zhang, J. Combination of Cation Exchange and Quantized Ostwald Ripening for Controlling Size Distribution of Lead Chalcogenide Quantum Dots. *Chem. Mater.* **2017**, *29*, 3615–3622.
- (38) Li, C.; Sato, R.; Kanehara, M.; Zeng, H.; Bando, Y.; Teranishi, T. Controllable polyol synthesis of uniform palladium icosahedra: effect of twinned structure on deformation of crystalline lattices. *Angew. Chem., Int. Ed. Engl.* **2009**, 48, 6883–6887.
- (39) Xia, Y.; Gilroy, K. D.; Peng, H. C.; Xia, X. Seed-Mediated Growth of Colloidal Metal Nanocrystals. *Angew. Chem., Int. Ed.* **2017**, *56*, 60–95.
- (40) Thanh, N. T. K.; Maclean, N.; Mahiddine, S. Mechanisms of nucleation and growth of nanoparticles in solution. *Chem. Rev.* **2014**, *114*, 7610–7630.
- (41) Wang, F.; Richards, V. N.; Shields, S. P.; Buhro, W. E. Kinetics and Mechanisms of Aggregative Nanocrystal Growth. *Chem. Mater.* **2013**, *26*, 5–21.
- (42) Yang, T. H.; Peng, H. C.; Zhou, S.; Lee, C. T.; Bao, S.; Lee, Y. H.; Wu, J. M.; Xia, Y. Toward a quantitative understanding of the

reduction pathways of a salt precursor in the synthesis of metal nanocrystals. *Nano Lett.* **2017**, *17*, 334–340.

- (43) Zhang, Z.; Wang, Z.; He, S.; Wang, C.; Jin, M.; Yin, Y. Redox reaction induced Ostwald ripening for size- and shape-focusing of palladium nanocrystals. *Chem. Sci.* **2015**, *6*, 5197–5203.
- (44) Zheng, Y.; Zeng, J.; Ruditskiy, A.; Liu, M.; Xia, Y. Oxidative etching and its role in manipulating the nucleation and growth of noble-metal nanocrystals. *Chem. Mater.* **2014**, *26*, 22–33.
- (45) Wiley, B. J.; Xiong, Y.; Li, Z. Y.; Yin, Y.; Xia, Y. Right bipyramids of silver: a new shape derived from single twinned seeds. *Nano Lett.* **2006**, *6*, 765–768.
- (46) Patala, S.; Marks, L. D.; Olvera De La Cruz, M. Elastic strain energy effects in faceted decahedral nanoparticles. *J. Phys. Chem. C* **2013**, *117*, 1485–1494.

□ Recommended by ACS

Synergy between Structure Characteristics and the Solution Chemistry in a Near/Non-Equilibrium Oxidative Etching of Penta-Twinned Palladium Nan...

Xiaoming Ma, Chuanhong Jin, et al.

FEBRUARY 08, 2021

THE JOURNAL OF PHYSICAL CHEMISTRY C

READ 🗹

Insights into Transformation of Icosahedral PdRu Nanocrystals into Lattice-Expanded Nanoframes with Strain Enhancement in Electrochemical Redox Reac...

Chen-Rui Kao, Chun-Hong Kuo, et al.

FEBRUARY 14, 2022

CHEMISTRY OF MATERIALS

READ **C**

Improving the Purity and Uniformity of Pd and Pt Nanocrystals by Decoupling Growth from Nucleation in a Flow Reactor

Ruhui Chen, Younan Xia, et al.

MAY 03, 2021

CHEMISTRY OF MATERIALS

READ 🗹

Pentacoordinate Al $^{3+}$ Sites Anchoring Synthesis of Palladium Intermetallic Catalysts on Al $_2$ O $_3$ Supports

Wen-Zhong Jiao, Hai-Wei Liang, et al.

APRIL 24, 2022

INORGANIC CHEMISTRY

READ 🗹

Get More Suggestions >